RSC Advances

PAPER

View Article Online
View Journal | View Issue

Cite this: *RSC Adv.*, 2023, **13**, 9715

A new strategy for improving cytotoxicity of a copper complex toward metastatic melanoma cells unveiled by EPR spectroscopy†

Eduardo Guimarães Vieira, [ab] Rodrigo Boni Fazzi,[a] Daniel O. T. A. Martins, [b] Alena M. Sheveleva,[b] Floriana Tuna *[b] and Ana Maria da Costa Ferreira *[a]

Received 15th November 2022
Accepted 20th March 2023

DOI: 10.1039/d2ra07266a

rsc.li/rsc-advances

A novel strategy of improving cytotoxicity against metastatic melanoma cells using an oxindolimine copper(II) complex immobilized and dimerized on a modified Polyhedral Oligomeric Silsesquioxane (POSS) matrix was developed, as revealed by electron paramagnetic resonance (EPR) spectroscopy. An assured correlation between continuous-wave (CW) and pulsed EPR spectroscopies provided a complete characterization of the actual active species, its coordination environment, as well as the efficiency/selectivity of the bioconjugate materials.

In the recent advanced development of metallodrugs beyond the traditional and approved platinum complexes,[1] copper compounds have deserved a special interest among other stimuli-responsive metal complexes.[2] Besides having redox activity that improves its cytotoxicity *versus* tumour cells, copper centres are often coordinated to biologically active ligands such as imines, triazoles or dithiocarbamates[3,4] that stabilize their oxidation states, frequently acting as antioxidants or inhibitors of selected proteins in a synergistic effect.[5] A common strategy to modify and improve its cytotoxicity is inserting them into inorganic nanoporous materials that can contribute significantly to its biological activities.[6–8]

EPR spectroscopy is particularly valuable for the characterization of metal complexes, allowing the determination of oxidation states, and the coordination environment around the metal centre.[9,10] Applications of this technique can provide powerful tools for understanding the diverse mechanisms of action of metal-based anticancer compounds,[11] contributing to the development of new medicinal agents.[12]

Here, we report a new approach for selective cytotoxicity towards metastatic melanoma cells through a surprising dimerization of an oxindolimine copper(II) complex immobilized on the surface of modified Polyhedral Oligomeric Silsesquioxane (POSS) nanoparticles, as demonstrated by Electron Paramagnetic Resonance (EPR) spectroscopy. At first, the idea was to extend the previous toxicity studies of imine copper(II) complexes with significant antiproliferative activity already observed toward human neuroblastoma cells (SH-SY5Y),[13] and melanoma cells[14] (murine B16F10 and human TM1MNG3).

In these previous studies, binuclear species were more efficient than the analogous mononuclear complexes toward melanomas (SKMEL-05 and SKMEL 147), and additional investigations demonstrated that the activity of such complexes depends on the melanin content in the cells, stimulated by UV radiation.[15] We also observed that the complex [*N*,*N*′[bis-(3,3′-indolin-2-one)]-1,3-diiminopropane]-copper(II), hereafter named as compound **1**, [Cu(isapn)]ClO_4 (Fig. S1, ESI†), showed selective activity toward metastatic melanoma cells (SKMEL-147) when immobilized on the surface of mesoporous silica matrices (MCM, and functionalized MCM-atzac).[6]

The complex used in the present study is the same compound **1** (see structure in Fig. S1 ESI†) of these previous investigations. It has been prepared and characterized by different spectroscopic techniques,[16] and showed pro-apoptotic properties toward different tumor cells.[17] The highlight of the current work is a new inactive matrix based on modified-POSS nanoparticles, where the cytotoxic effect is only owed to inserted complex species. On the contrary, in the case of MCM, the matrices also contributed to the cytotoxicity of the copper(II) complex.

Herein, complex **1** was inserted into a non-active modified-POSS matrix, hexa[(3-amino-1,2,4-triazole-5-carboxylic acid) dichloropropyl] octasilsesquioxane (POSS-atzac), giving rise to a new bioconjugate material, hereafter referred to as compound **2**, POSS-atzac-[Cu(isapn)] (Fig. 1). The free-metal POSS-atzac matrix is diamagnetic and has been therefore characterized by ^{13}C and ^{29}Si solid state-NMR (see Fig. S2 ESI†). By contrary, the bioconjugate compound **2** is paramagnetic due to presence of copper(II). Interestingly, its antiproliferative activity against

[a]*Department of Fundamental Chemistry, Institute of Chemistry, University of São Paulo, 05508-000 São Paulo-SP, Brazil. E-mail: amdcferr@iq.usp.br*

[b]*EPSRC National EPR Facility, Department of Chemistry and Photon Science Institute, University of Manchester, Manchester M13 9PL, UK. E-mail: floriana.tuna@manchester.ac.uk*

† Electronic supplementary information (ESI) available: Supporting Fig. S1–S3. See DOI: https://doi.org/10.1039/d2ra07266a

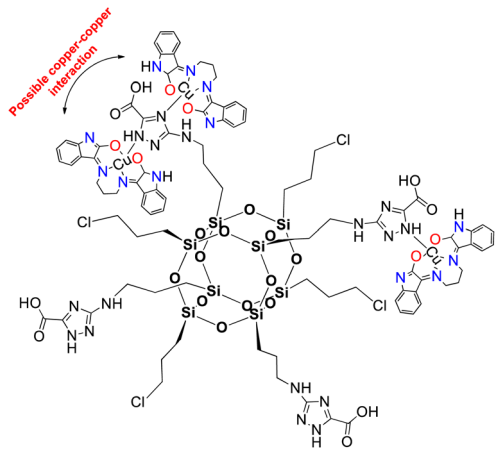

Fig. 1 Representation of [Cu(isapn)] complex immobilized in the modified-POSS matrix, compound **2**. Indolinone nitrogen and oxygen atoms are highlighted in blue (N) and red (O) respectively.

SKMEL-147 cancer cells demonstrated a higher cytotoxicity compared to both complex **1** and pure modified-POSS. Additionally, this new material showed enhanced selectivity that is at least twice greater after 24 h and three times greater in 48 h incubation, compared to the non-tumour cell line fibroblast P4 (see Table S1 ESI†).

To identify the source of such significant improvement in the reactivity of bioconjugate material **2**, we have performed continuous-wave and pulsed EPR measurements on both **1** and **2**, given EPR is powerful in identifying paramagnetic ions and in probing potential modifications in the environment of copper(II).

X-band CW-EPR spectrum of **2** at room and low temperature (10 K) confirmed the insertion of **1** onto the surface-modified POSS (Fig. 2). The signal can be modelled considering a mononuclear copper(II) species with $g_{xy} = 2.065(1)$, $g_z = 2.271(1)$ and $\boldsymbol{A}_z^{Cu} = 157$ G (500 MHz) $= 166.4 \times 10^{-4}$ cm^{-1}, giving $g_{\|}/A_{\|} =$ 136 cm. In previous studies, the parameters for the free complex **1** in frozen methanol : water solution (4 : 1 v/v) at 77 K were determined as $g_{xy} = 2.091$, $g_z = 2.301$, $\boldsymbol{A}_{xy}^{Cu} = 14.2$ G, $\boldsymbol{A}_z^{Cu} = 111.5$ G $= 126 \times 10^{-4}$ cm^{-1}, and ratio $g_{\|}/A_{\|} = 183$ cm, indicating a distorted tetrahedral environment around copper ion.[16] Differences in *g*- and *A*-tensors for **2** confirm that the observed spectrum is due to the inclusion of **1** on the surface instead of dispatched **1.**

Further evidence of insertion of **1** on POSS in **2** could be found in CW spectra analysis. The nitrogen hyperfine is smaller than the linewidth, but the *xy* component can be extracted from the derivative of the CW signal (second harmonic, Fig. 3). It can be simulated considering four equivalent nitrogen-14 nuclei with $\boldsymbol{A}_{xy}^{N} = 49$ MHz (17 G). We attribute these signals to nitrogen donor-atoms bonded to the equatorial plane of copper(II) arise due to the binding to triazole fragment.[6]

As the sample is cooled to 10 K, a weak signal appears around 160 mT. This signal is assigned to a forbidden $\Delta m_s = \pm 2$ transition which usually indicates presence of species with $S >$ 1/2 species, indicative that some magnetic interactions between copper entities may occur within the hybrid material.[14] The forbidden transitions get partially relaxed when the energy levels are not degenerated at zero magnetic due to the presence of zero-field splitting (ZFS) interactions. Hence, this signal can be reproduced considering a spin triplet ($S = 1$) that may arise from magnetic interaction between adjacent copper(II) ions, using the spin Hamiltonian (1).

$$\hat{H} = \mu_B \boldsymbol{B}\boldsymbol{g}\hat{\boldsymbol{S}} + D\left(\hat{S}_z^{\,2} - S(S+1)/3\right) + E\left(\hat{S}_x^{\,2} - \hat{S}_y^{\,2}\right) \quad (1)$$

where the coefficients D and E are the axial and rhombic ZFS parameters respectively and the ratio E/D lies between 0 and 1/3, the other symbols have their usual meaning. As the overall spectrum is dominated by the contributions of non-interacting copper(II) ($S = 1/2$), it is difficult to assess with accuracy the

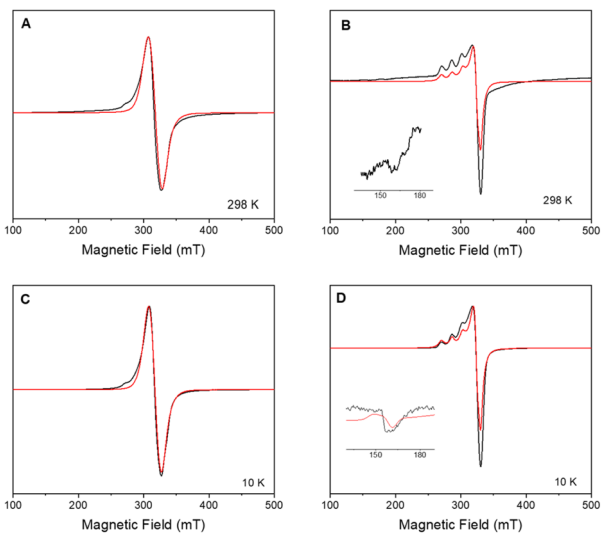

Fig. 2 Experimental (black) and simulated (red) X-band CW-EPR spectra of polycrystalline compound **1** at (A) 298 K, and (C) 10 K; and compound **2** at 298 K (B) and 10 K (D). Inset in (B) and (D) show the half-field region, with simulation in red. Parameters are provided in the text.

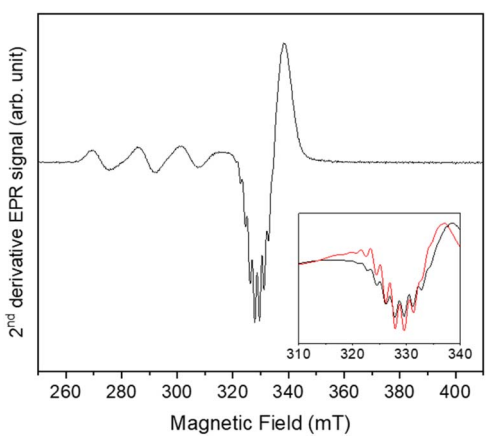

Fig. 3 Second harmonic X-band CW-EPR spectrum of compound **2** at 50 K (black) and its simulation (red). Inset shows the simulation of the g_{xy} region, evidencing hyperfine couplings with ^{63,65}Cu and ^{14}N.

percentage of dimerized species. The half-field transition is satisfactorily reproduced with eqn (1) and D in the range 0.03–0.05 cm^{-1} and E 0.001–0.01 cm^{-1}.

Interaction between copper(II) ions in **2** is not unexpected given the flexibility of the aliphatic arms of POSS, resulting in oligomers as attested by EPR spectroscopy. Based on this evidence, it is assumed that the binuclear compound is the actual active species, since the free complex or non-metalated modified-POSS matrices did not show substantial anti-proliferative activities against SKMEL-147 cancer cells[6] (see also Table S1 at ESI†).To test this possibility, a mimetic binuclear complex [Cu(isapn)(μ-triazole) Cu(isapn)] (see Fig. 4) was prepared and its EPR was measured in similar experimental conditions. Notably, comparable EPR parameters to compound **2**, $g_{xy} = 2.060(1)$, $g_z = 2.268(1)$ and $A_z = 458$ MHz (145 G), were obtained by simulation.

To better determine the metal coordination environment of [Cu(isapn)](ClO_4) complex loaded on the matrix surface, Hyperfine Sublevel Correlation (HYSCORE) spectroscopy[18] was carried out on **1** and **2** at 5 K, at a magnetic field correspondent to the maximum intensity of the echo-detected field-sweep (EDFS) spectrum as shown in Fig. S4 (ESI†).

In HYSCORE spectroscopy, when the nucleus is weakly coupled to the electron, meaning that the hyperfine coupling is less than twice the nuclear Larmor frequency ($|A| < 2\nu$), the signals appear in the (+, +) quadrant, are centred on the nuclear Larmor frequency and spread by the hyperfine coupling along the antidiagonal. On the other hand, when the nucleus is strongly coupled, *i.e.* $|A| > 2\nu$, the transitions appear in the (−, +) quadrant, they are centred on half the hyperfine and spread along the diagonal by twice the Larmor frequency.

The presented HYSCORE spectra were detected at the maximum of echo intensity. Thus, for compound **1** the spectrum shown on Fig. 5A is dominated by signals from nitrogen-14 nuclei. It can be reproduced according to spin Hamiltonian (2).[19]

$$\hat{H} = \mu_B \boldsymbol{B} \boldsymbol{g} \hat{\boldsymbol{S}} - \sum_i \mu_n g_{ni} \boldsymbol{B} \hat{\boldsymbol{I}}_i + \sum_i \hat{\boldsymbol{S}} \boldsymbol{A}_i \hat{\boldsymbol{I}}_i + \sum_i \hat{\boldsymbol{I}}_i \boldsymbol{P}_i \hat{\boldsymbol{I}}_i \qquad (2)$$

where $S = 1/2$ is the electronic spin of the complexes, μ_B is the Bohr magneton, → the compound's g-tensor and $\boldsymbol{B}$ is the magnetic field vector. The subscript i refers to the different spin-active nuclei. $\boldsymbol{I}_N = 1$ is the nuclear spin of ^{14}N (99.6% natural abundance), $\boldsymbol{A}$ is the hyperfine tensor, μ_n is the nuclear magneton, g_n is the nuclear g-value $\boldsymbol{P}_N$ is the nuclear quadrupole interaction tensor of nitrogen nucleus, described in (3),

$$\boldsymbol{P}_N = \begin{pmatrix} P_1 & 0 & 0 \\ 0 & P_2 & 0 \\ 0 & 0 & P_3 \end{pmatrix} = \frac{e^2 Q_N \boldsymbol{q}/h}{4I_N(2I_N - 1)} \begin{pmatrix} -(1-\eta) & 0 & 0 \\ 0 & -(1+\eta) & 0 \\ 0 & 0 & 2 \end{pmatrix} \qquad (3)$$

where $Q_N = +0.02044(3)$ barn is the scalar quadrupole moment of nitrogen-14, e is the elementary charge, the parameters eQ and $e\boldsymbol{q}$ are the contributions from nuclear quadrupole moment and electric field gradient respectively and the quantity $e^2Q\boldsymbol{q}/h$ is the quadrupole coupling constant in MHz, η is the asymmetry parameter and the other symbols have their usual meaning.[20] The quadrupole coupling constant ($e^2Q\boldsymbol{q}/h$) can be estimated from the position of the ridges according to (4),

$$\nu^{DQ}_{\alpha,\beta} = 2\sqrt{\left(\nu \pm \frac{A}{2}\right)^2 + \left(\frac{e^2qQ}{4h}\right)^2 (3 + \eta^2)} \qquad (4)$$

where ν^{DQ} are the frequencies of the double-quantum transitions, ν is the Larmor frequency of the corresponding nuclei and the other symbols have the usual meaning. Knowing that the asymmetry parameter's (η) lower and upper limits are 0 and 1 respectively, eqn (4) gives a range of $e^2Q\boldsymbol{q}/h$.[21]

For **1**, the signal is mainly observed in the (−, +) quadrant at about [−2.6, 5.8], [−5.8, 2.6] MHz with a separation of *ca.* 3.2

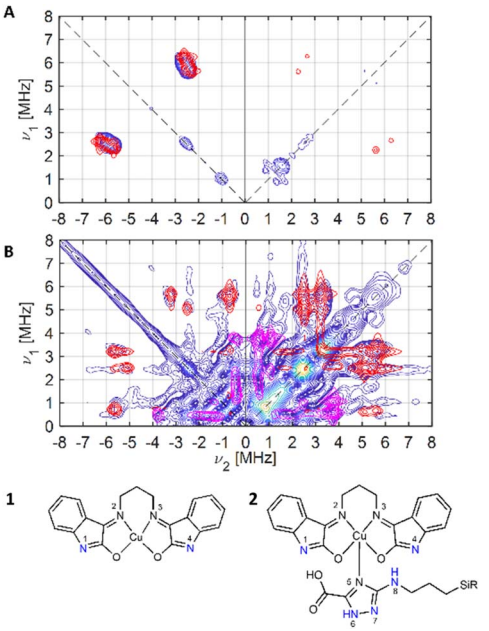

Fig. 5 Experimental (blue) and simulated (red: N1, N4; magenta: $N_{triazole}$ (N6, N7)) X-band ^{14}N HYSCORE spectra of (A) compound **1** and (B) compound **2**, schematically represented below.

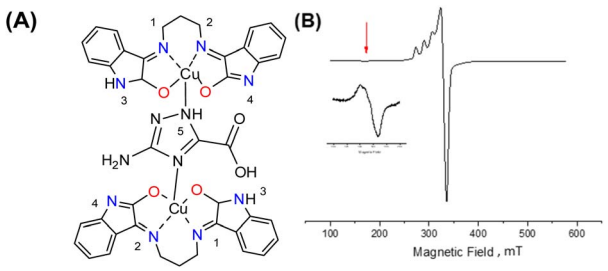

Fig. 4 (A) Molecular structure of the mimetic binuclear complex [Cu(isapn)(μ-triazole)Cu(isapn)]; (B) X-band CW EPR spectrum of this binuclear complex measured on solid-state samples at room temperature; also showing the signal at 150 mT corresponding to an interaction between two copper centres.

MHz, which corresponds to the hyperfine A^{N}_{xyz} = 3.9, 3.2, 3.2 MHz ($A^{N}_{iso} \sim 3.4$ MHz). This set of signals has a nuclear quadrupole coupling parameter, e^2Qq/h, of 2.6 MHz and asymmetry parameter, η, of 0.

The magnitude of the hyperfine suggests that the observed cross-peaks in Fig. 5A stem from the remote nitrogen atoms N1 and N4 (Fig. 5) because stronger couplings are expected for directly bonded nitrogen.[22,23] The hyperfine interactions of N2 and N3 should lie in a strongly coupled range (~45 MHz) and cannot be detected in HYSCORE.[23] In CW EPR spectrum of **1** this super hyperfine splitting is masked by the broadening of the linewidth in solid state (Table 1).

The HYSCORE spectrum of the hybrid compound **2**, POSS-atzac-[Cu(isapn)] is characterized by cross peaks in both the (+, +) and (−, +) quadrants, arising from transitions associated with the remote nitrogen-14 nucleus (Fig. 5B) and can be reproduced according to the spin Hamiltonian (2) assuming two distinct signals in the Poss-immobilized sample.

In contrast to compound **1** HYSCORE spectrum of compound **2** shows elongated cross peaks appearing at low frequency range [±0.5, +3.5], [±3.5, +0.5], [±2.5, +0.5], and [±0.5, +2.5] MHz, which correspond to the hyperfine A^{N}_{xyz} = 1.5, 1.7, 1.7 MHz ($A^{N}_{iso} \sim 1.6$ MHz), a nuclear quadrupole coupling $e^2Qq/h = 1$ MHz, and an asymmetry parameter, η, of 0.85. Such values are typical for remote ^{14}N atoms in metal ion coordinated imidazoles reported by Mims and Peisach.[24] This together with observed in CW super-hyperfine splitting allow us to assign these transitions to remote nitrogen of triazole ligand N6 or N7 (Fig. 5B). In addition to these signals we observe cross peaks at about [−5.6, 0.8], [−0.8, 5.6], [±5.6, +3.3], [±3.3, +5.6], [±5.0, +2.5] and [±2.5, +5.0] MHz. The simulation showed reasonable agreement using to the hyperfine of A^{N}_{xyz} = 2.7, 2.2, 2.2 MHz ($A^{N}_{iso} \sim 2.4$ MHz), a nuclear quadrupole coupling $e^2Qq/h = 3.8$ MHz, and an asymmetry parameter, η, of 0.32. This can be assigned again to the remote N1 and N4 atoms (Fig. 5B) and the reduction of hyperfine value with increase of quadrupole coupling and asymmetry can be attributed to the covalent bonding of compound **1** to triazole ligand in **2**.[22]

Additional results were obtained and added to ESI.† In Fig. S4,† echo-detected absorption spectra for pure complex **1** in solution, and immobilized copper(II) species in solid complex **2**, measured at 5 K, are displayed. Spin–lattice relaxation time (T_1) for [Cu(isapn)]ClO_4 **1** and POSS-atzac-[Cu(isapn)] **2** were determined at three different fields at 5 K, as shown in Fig. S5 ESI.† Long T_1 values were found for both compounds, varying from 145 to 867 μs for 1 and 940 to 1540 μs for **2**. The longer relaxation time in 2 is likely due to the higher magnetic dilution provided by the diamagnetic POSS matrix. Finally, two-pulse electron spin echo decays for complexes **1** and **2** were measured at three different fields (Fig. S6 and S7 ESI†). Again, Longer T_2 times of 0.95–1.19 μs were observed for **2**, compared to 0.56–0.67 μs for **1**. In addition, the echo decay traces are marked by strong nuclear modulation due to ^{14}N, further confirming the binding of additional triazole nitrogen to Cu(II) in the hybrid material.

In short, the data described in this work made it possible to understand the increase in the cytotoxicity of supported compound **2** regarding free complex **1**, due to the formation of a binuclear species that are more reactive than the corresponding mononuclear one (Fig. 2, and S3 ESI†).

These results can help in establishing a new approach to obtain efficient and selective cytotoxic agents against melanoma cells. According to our knowledge, this is the first time where modified nuclearity of metal species was verified by EPR spectroscopy inside a modified-Polyhedral Oligomeric Silsesquioxane (POSS) matrix. Further relevant results complementing these preliminary data will be reported in due course.

Table 1 Extracted HYSCORE parameters from simulations

	A_{xyz}[a] (MHz)	A_{iso}[a] (MHz)	e^2Qq/h (MHz)	η	Compounds
N1, N4	3.9, 3.3, 3.3	~3.5	2.6	0.00	**1**
N1, N4	2.7, 2.2, 2.2	~2.4	3.8	0.32	**2**
$N_{triazole}$	1.5, 1.7, 1.7	~1.6	1.0	0.85	**2**

[a] N2, N3 and N5 were not detected.

Conflicts of interest

There are no conflicts of interest to declare.

Acknowledgements

This work was financially supported by the São Paulo State Research Foundation (FAPESP, grants 2016/16735-8 and 2017/21919-3), FAPESP/Sprint Project USP-EPSRC/University of Manchester (grant 2016/50342-3), and CEPID-Redoxoma Network (FAPESP, grant 2013/07937-8). The authors acknowledge the EPSRC UK National EPR Facility at the University of Manchester for EPR measurements (NS/A000055/1 and EP/W014521/1). We further thank The University of Manchester (UK) for a President's Doctoral Scholarship award to D. O. T. A. M. and research internships to E. G. V. and R. B. F.

Notes and references

1 R. G. Kenny and C. J. Marmion, *Chem. Rev.*, 2019, **119**, 1058–1137.
2 X. Wang, X. Wang, S. Jin, N. Muhammad and Z. Guo, *Chem. Rev.*, 2019, **119**, 1138–1192.
3 C. Santini, M. Pellei, V. Gandin, M. Porchia, F. Tisato and C. Marzano, *Chem. Rev.*, 2014, **114**, 815–862.
4 S. A. Andres, K. Bajaj, N. S. Vishnosky, M. A. Peterson, M. S. Mashuta, R. M. Buchanan, P. J. Bates and C. A. Grapperhaus, *Inorg. Chem.*, 2020, **59**, 4924–4935.
5 L. Brustolin, C. Nardon, N. Pettenuzzo, N. Zuin Fantoni, S. Quarta, F. Chiara, A. Gambalunga, A. Trevisan, L. Marchiò, P. Pontisso and D. Fregona, *Dalton Trans.*, 2018, **47**, 15477–15486.
6 E. Guimarães Vieira, R. B. Miguel, D. Rodrigues Da Silva, R. Boni Fazzi, R. A. A. De Couto, J. H. Marin, M. L. A. Temperini, J. Da Silva Shinohara, H. E. Toma,

L. C. Russo, Y. T. Magalhães, N. L. Dias Filho, F. L. Forti and A. M. Da Costa Ferreira, *New J. Chem.*, 2019, **43**, 386–398.
7 C. He, D. Liu and W. Lin, *Chem. Rev.*, 2015, **115**, 11079–11108.
8 H. Chen, D. Liu and Z. Guo, *Chem. Lett.*, 2016, **45**, 242–249.
9 D. T. Petasis and M. P. Hendrich, *Methods Enzymol.*, 2015, **563**, 171–208.
10 A. Abragam, and B. Bleaney, *Electron Paramagnetic Resonance of Transition Ions*, Oxford University Press, Oxford, 2012.
11 J. Eisermann, M. Seif-Eddine and M. M. Roessler, *Curr. Opin. Chem. Biol.*, 2021, **61**, 114–122.
12 K. E. Prosser and C. J. Walsby, *Eur. J. Inorg. Chem.*, 2017, 1573–1585.
13 G. Filomeni, G. Cerchiaro, A. M. Da Costa Ferreira, A. De Martino, J. Z. Pedersen, G. Rotilio and M. R. Ciriolo, *J. Biol. Chem.*, 2007, **282**, 12010–12021.
14 C. J. Nunes, B. E. Borges, L. S. Nakao, E. Peyroux, R. Hardré, B. Faure, M. Réglier, M. Giorgi, M. B. Prieto, C. C. Oliveira and A. M. Da Costa Ferreira, *J. Inorg. Biochem.*, 2015, **149**, 49–58.
15 C. J. Nunes, A. H. Otake, S. O. Bustos, R. B. Fazzi, R. Chammas and A. M. Da Costa Ferreira, *Chem.-Biol. Interact.*, 2019, **311**, 108789.
16 G. Cerchiaro, P. L. Saboya, A. M. Da Costa Ferreira, D. M. Tomazela and M. N. Eberlin, *Transition Met. Chem.*, 2004, **29**, 495–504.
17 G. Cerchiaro, K. Aquilano, G. Filomeni, G. Rotilio, M. R. Ciriolo and A. M. Da Costa Ferreira, *J. Inorg. Biochem.*, 2005, **99**, 1433–1440.
18 A. G. Maryasov and M. K. Bowman, *J. Phys. Chem. B*, 2004, **108**, 9412–9420.
19 J. Telser, *eMagRes*, 2017, vol. 6, pp. 207–234.
20 S. Stoll and D. Goldfarb, *eMagRes*, 2017, vol. 6, pp. 495–510.
21 S. Van Doorslaer, in *eMagRes*, John Wiley & Sons, Ltd, Chichester, UK, 2017, vol. 6, pp. 51–70.
22 M. Iwaizumi, T. Kudo and S. Kita, *Inorg. Chem.*, 1986, **25**, 1546–1550.
23 F. Neese, *J. Phys. Chem. A*, 2001, **105**, 4290–4299.
24 W. B. Mims and J. Peisach, *J. Chem. Phys.*, 1978, **69**, 4921–4930, DOI: **10.1063/1.436479**.